Experimental limit for the circular polarization of the 1081 keV gamma ray in ^{18}F

M. Bini, T. F. Fazzini, G. Poggi, and N. Taccetti
Department of Physics, Università di Firenze, 50125 Firenze and Istituto Nazionale di Fisica Nucleare, 50125 Firenze, Italy
(Received 5 April 1988)

A measurement of the circular polarization P_γ of the 1081 keV γ-ray in ^{18}F is reported. The result is $P_\gamma=(2.7\pm5.7)\times10^{-4}$. The reaction used was ^{16}O(^{3}He,p)^{18}F with a 3.4 MeV ^{3}He$^+$ beam of an intensity of 7 μA impinging on a windowless water target. The circular polarization was measured with a four-prong transmission-type Compton polarimeter. The measurement of the analyzing power of the polarimeter is presented. Gamma rays were detected by means of 130 cm^3 p-type germanium detectors placed behind the prongs. Four independent data acquisition channels were used: pile-up losses at a counting rate of 60 kcps were kept lower than 15%, owing to the use of trapezoidal shapers. Systematic effects of instrumental origin are discussed and found to give negligible contributions with respect to the statistical uncertainty. The calculation of the asymmetries is performed using different estimators; an extensive comparison of the various methods is presented. The result of the experiment, when averaged with those of the other experiments on ^{18}F carried out until now, gives a grand average $P_\gamma=(1.2\pm3.9)\times10^{-4}$. This result is compared with recent theoretical estimates.

I. INTRODUCTION

The measurement of the circular polarization P_γ of the 1081 keV γ ray deexciting the first $J^\pi=0^-$, $T=0$ state in ^{18}F has been the subject of much experimental work in recent years.[1-6] In fact it was recognized as one of the most direct ways of studying the effect of neutral weak currents between hadrons. The circular polarization P_γ comes out from the mixing of the parity doublet (1042 keV, $J^\pi=0^+$, $T=1$; 1081 keV, $J^\pi=0^-$, $T=0$) in ^{18}F (see Fig. 1). The mixing is induced by the isovector part ($\Delta T=1$) of the parity nonconserving weak nucleon-nucleon (N-N) potential. As was extensively reviewed in Ref. 1, a remarkable experimental as well as theoretical effort was devoted to circumvent the problem associated with the lack of a detailed knowledge of nuclear wave functions in ^{18}F. In the hypothesis that a dominant contribution to the $\Delta T=1$ part of the weak parity nonconserving potential comes out from the term due to one-pion exchange, it was possible to find a substantially model-independent relation between circular polarization P_γ and coupling constant f_π of the weak πNN vertex: $|f_\pi|=(2.3\pm0.4)\times10^{-4}|P_\gamma|$.

Until 1981, theoretical calculations[7,8] set a broad range of possible values of f_π between 2×10^{-7} and 11×10^{-7}. Later Desplanques, Donoghue, and Holstein (DDH) (Ref. 9) proposed a range of possible values of f_π from 0 to 9×10^{-7} with a best value: $f_\pi^{\rm DDHbv}=4.6\times10^{-7}$, so that the expected theoretical range for $|P_\gamma|$ was $0-48\times10^{-4}$, with a best value $|P_\gamma|^{\rm DDHbv}=20\times10^{-4}$. A first series of three experiments[2-4] gave an average value of $P_\gamma=(-8\pm12)\times10^{-4}$, which at one standard deviation confidence level excluded values of f_π larger than $\approx4.6\times10^{-7}$. More recently, two new measurements of P_γ, performed at Queen's University[1,6] and at the University of Florence,[5] lowered substantially the uncertainty in the measurement of P_γ. Results of the experiment carried out in our laboratory have already been reported in a previous letter:[5] in this paper we give a more extensive presentation of the experimental procedures and of the data analysis. Moreover, the comparison between experimental results and theoretical predictions is extended to the more recent theoretical calculations performed by Dubovik and Zenkin (DZ),[10] by Desplanques[11] and Kirchbach.[12]

In Sec. II a description of the apparatus is given; in Sec. III the systematic effects are discussed and an estimate of their influence on the asymmetry is calculated. Section IV presents the procedures adopted for the calculation of the asymmetry of the 1081 keV γ line.

II. EXPERIMENTAL SETUP

The circular polarization P_γ (1081 keV) is experimentally determined by measuring the asymmetry A in the counts N of the 1081 keV photopeak associated to opposite magnetization states of equal duration of a transmission-type Compton polarimeter. This is done according to the relation $P_\gamma=A/S$, where S is the analyzing power of the polarimeter and A is, in principle, defined as

$$A=\frac{N^\uparrow-N^\downarrow}{N^\uparrow+N^\downarrow},$$

where the arrows refer to the direction of the oriented electron spin relative to the γ-ray propagation vector, upward arrow indicating parallel, downward arrow indicating antiparallel direction.

With respect to a previous experiment performed in our laboratory,[3] special efforts have been devoted to improve the experimental conditions: the improvements concerned the target, the polarimeter, the linear shaping

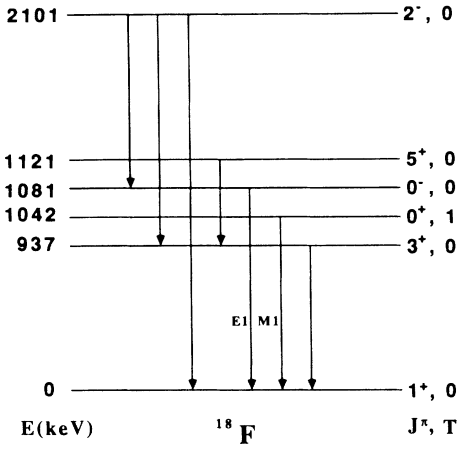

FIG. 1. Level scheme of ^{18}F; only levels relevant to the present experiments are shown.

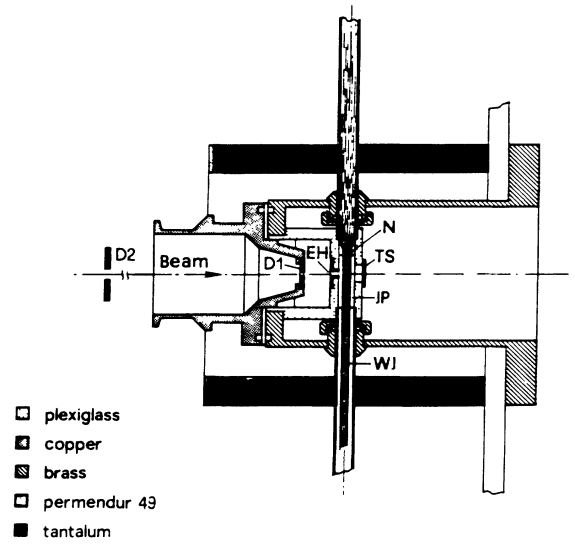

FIG. 2. Windowless water target. $D1$-$D2$, beam diaphragms; EH, entrance hole; TS, Tantalum stopper, N, nozzle; JP, water jet pipe; WJ, water jet.

of the signals, and the data acquisition system: these points are discussed later in this section.

A. Windowless water target

In all the experiments performed until now[1-6] ^{18}F was populated via the ^{16}O(^{3}He,p) reaction at $E(^3\text{He})=3-3.7$ MeV. Currents of the order of 5–15 μA were necessary to get the desired statistical accuracy in a reasonable running time (a few months of beam on target). A problem encountered in these experiments is the oxygen target which is to be thick and at the same time capable of withstanding the power deposited by the beam. In Ref. 3 a solid quartz target was used. Currents as high as 5 μA were sustained by the target; however, effects related to the oxygen contents of the quartz were observed, i.e., at high beam currents the target yield was poorer than at low current. Circulating water targets have been used in Refs. 2, 4, and 6. These targets made it possible to remove the activity associated with the ground-state (g.s.) β^+ decay of ^{18}F while no problems about the high current yield were reported. However, in all these experiments a metal foil was used in order to decouple the water from the vacuum system. Nickel and titanium foils were used, and in some cases, in order to increase the lifetime of the window, the beam was spread over a larger area: lifetimes of the order of two days were reported. The use of a window poses problems because of the deterioration of the γ line shape as Ge detectors become more and more damaged by neutrons from the ^{12}C(^{3}He,n) reaction on the carbon deposit on the window. Moreover, the carbon buildup leads to a time-dependent background underlying the lines of interest. To overcome these problems a water stream target was implemented with a technique similar to that used in differential pumping gas targets: i.e., a target with no window between water stream and vacuum of the beam line. The mechanics of the target are reported in Fig. 2 while a detailed description of its operation can be found in Ref. 13. In Fig. 3 a sketch of the whole assembly of the target and polarimeter is reported. The behavior of the target was tested with satisfactory results up to currents of 20 μA of ^{3}He$^+$ with an energy of 3.3 MeV. During the measurements ($I_{\text{He}}=7$ μA, $E_{\text{He}}=3.4$ MeV) no neutron damage effects on Ge detectors were observed.

B. Polarimeter

The mechanics of the four-prong polarimeter are shown in Fig. 4, where materials and dimensions are also specified. Each prong, made of Permendur 49, consisted of a cylindrical core (diameter 52 mm, length 61 mm) and a cylindrical head (diameter 64 mm, thickness 13 mm);

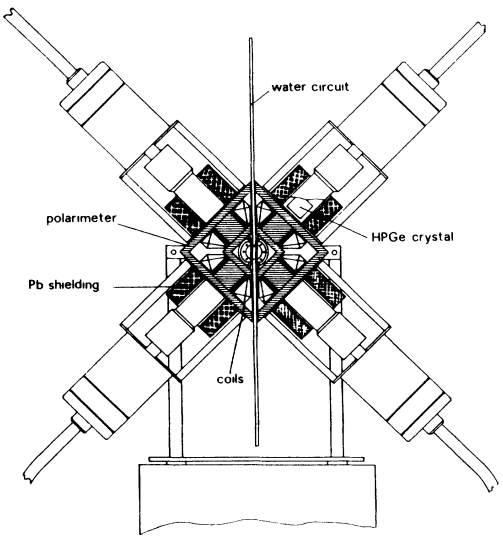

FIG. 3. Experimental setup. The water jet chamber is fitted inside the polarimeter.

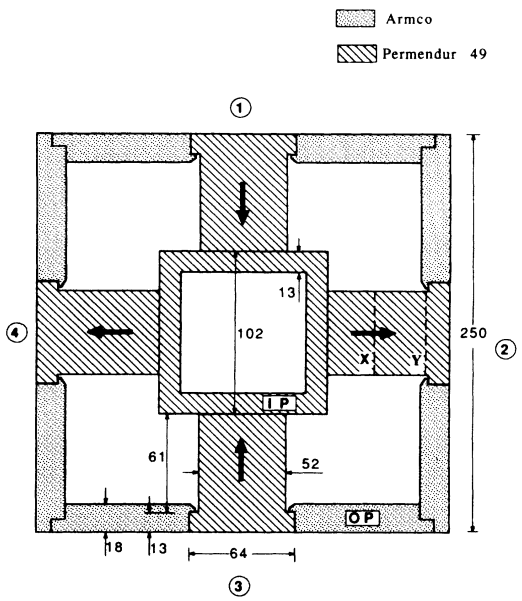

FIG. 4. Mechanics of the four-prong polarimeter. Dimensions are in mm.

the head is a part of the closing path of the magnetic induction flux. The closing path consisted of an inner path, labeled IP in Fig. 4, made of Permendur 49 and an outer path (labeled OP in Fig. 4) made of four sheets of ARMCO iron. Clearances within $\frac{1}{100}$ mm of the couplings between the prong heads and the ARMCO sheets were obtained by careful machining. The transversal dimension (140 mm) of the closing paths was chosen in such a way that the magnetization saturation would occur first in the prong cores. Magnetization was induced by four coils, wrapped around the cores, each of 93 turns of copper wire of rectangular section (2×4 mm^2). Coils were connected in series in such a way that the magnetization direction was as shown by the arrows in Fig. 4 in one phase of the operation and all reversed in the other phase. The phase reported in Fig. 4 is the one referred to as "+", while "−" will denote the opposite phase.

The switching between the two polarimeter phases was obtained by reversing the magnetizing current with a transistor bridge (transition time $\approx$400 ms); the induction flux variation $\Delta\Phi(B)$ was measured at each transition, by sending the current induced in a measure coil (100 turns copper wire) to an integrating amplifier. During the experiment the polarimeter was operated at a current of 21 A (magnetizing field of about 3.2×10^4 A turns/m) which corresponds to a measured induction field B of 2.24 T at position Y of Fig. 4. Measurements performed with the measuring coil placed at position X gave an induction field B 2% stronger than that at Y position [$B(X)=2.29$ T]. The identity, within the uncertainty of the measurement ($\pm0.25\%$), of the B field in the four prongs was also verified. In this situation measurements of stray field along the beam axis were made by means of a Hall probe. The probe (sensitivity of about 1 V/T, offset voltage instability of 10^{-5} V/K) made it possible to measure the field up to distances of about 40 cm away from the center of the polarimeter. A rough estimate of the bending of the $^3He^+$ beam of 3.4 MeV energy suggests a possible transversal beam motion at the target of about 2 μm. The same probe was used to measure the induction field at the Ge detectors position: a maximum induction field of 2×10^{-3} T was found in correspondence of the center of the end cup of the detectors.

C. Evaluation of the analyzing power of the polarimeter

The analyzing power of the polarimeter has been deduced from magnetic measurements as well as by means of γ sources of known circular polarization.

From the magnetic measurements reported in subsection B, the number Nf of aligned electrons per unit volume (N number of electrons per m^3, f fraction of aligned electrons) in the core, can be found by using an average value of $B=2.26$ T, as

$$Nf=1.91\times10^{29}\ \text{aligned electrons}/m^3\ .$$

Following Ref. 14, the analyzing power S at 1081 keV can be inferred to be

$$S(1081\ \text{keV})=Nf\sigma_c(1081\ \text{keV})[L_c+k(L_1+L_2)]\ ,$$

where σ_c is the part of the Compton scattering cross section dependent on the circular polarization of the γ rays, L_c is the geometrical length of the core (61 mm), L_1 and L_2 are the geometrical thicknesses of the end plates (13 mm each) and k a coefficient (smaller than 1) which takes into account the bending of the magnetization lines in the end plates as well as the different sections crossed by γ rays in the near and far end plates. The latter effect depends on the geometry of the experiment: relative position of the γ source, polarimeter, detector, and size of the polarimeter and of the detector. In Ref. 14, the analyzing power of a single-core polarimeter was measured and it was found that the measured value could be accounted for by taking $k=0.6\pm0.2$. Since the geometrical dimensions of that polarimeter are identical to those of a prong of the present polarimeter, and the geometrical configuration of the source and detectors is still very similar, we use this result to get a value

$$S(1081\ \text{keV})=(1.89\pm0.14)\times10^{-2}\ .$$

However, in order to have a direct information, we measured the analyzing power of one of the four prongs of the polarimeter by means of a source of γ rays of known circular polarization, placed at the target position. A ^{22}Na β source was used: in fact, the circular polarization of the 1274 keV γ rays, detected in coincidence with the positrons feeding the 1274 keV level in ^{22}Ne, is known to be

$$P_C=\frac{1}{3}\frac{v}{c}\cos\theta_{\beta\gamma}\ ,$$

where $\theta_{\beta\gamma}$ is the angle between the gamma and positron momenta and v is the positron velocity.

In Fig. 5 the experimental setup used in this measurement is reported. Positrons were detected with a surface

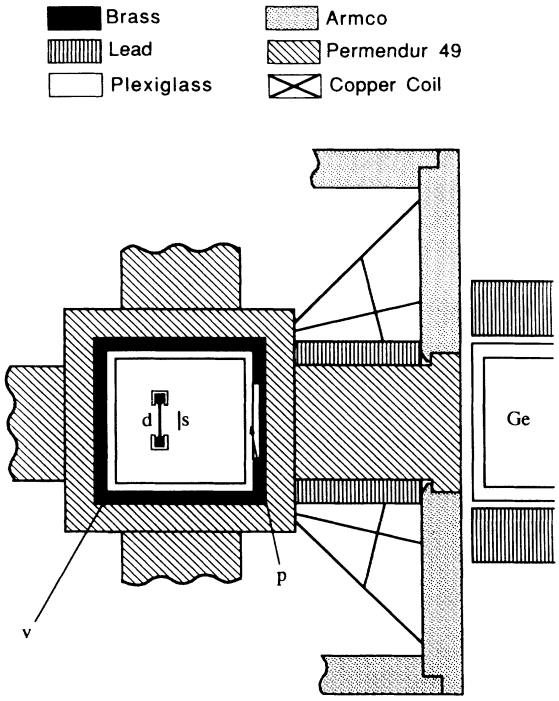

FIG. 5. Experimental setup for the measurement of the analyzing power of one prong of the polarimeter. v, vacuum chamber; p, Plexiglass lining; s, ^{22}Na β source; d, surface barrier silicon detector; Ge, HPGe detector.

barrier silicon detector of 200 mm^2 active area and 1 mm thickness. In order to keep the intensity of scattered positrons on surrounding materials low, for the detector the "transmission" mounting has been chosen and its metallic case, as well as the walls of the vacuum chamber, were lined with low Z materials (teflon and Plexiglass). Positron-gamma coincidences were recorded in the standard three-parameter mode (positron energy, γ energy, time difference) on magnetic tape and then analyzed offline. A total of 6.6×10^6 events in the full energy peak of the 1274 keV line were recorded in coincidence with positron pulses in the amplitude range 100–550 keV. The experimental asymmetry was found to be

$$A(1274\ \text{keV})=(4.4\pm0.4)\times10^{-3}\ ,$$

where the quoted error is a purely statistical one.

Following the procedure described in Ref. 14 we estimated

$$S(1081\ \text{keV})=(1.9\pm0.2)\times10^{-2}\ .$$

This is the value which will be adopted for extracting P_γ from the experimental asymmetry of the 1081 keV line.

D. Detectors

Detectors were hyperpure germanium (HPGe) of the p type. In Table I their efficiencies and geometrical dimensions are reported.

Possible effects due to stray magnetic field (see subsection B) on charge collection in Ge detectors were investigated. This has been done by placing one of the detectors, with a ^{60}Co source in front of it, in a magnetic field having a pattern similar to that of the polarimeter and an intensity of about 0.1 T at the detector position. By collecting the γ spectra associated with different signs of the field, it was possible to check the presence of spurious asymmetry. The linear electronics, the counting rate, and the accepted energy region (800–1500 keV) were the same as during the actual ^{18}F measurements. An asymmetry of $(1.5\pm1.5)\times10^{-5}$ was found for the total counts and of $(3.0\pm2.9)\times10^{-5}$ for the photopeaks energy regions. Taking into account that in the actual measurement the intensity of the field was more than a factor of 50 weaker, by linearly scaling one can guess a limit of 6×10^{-7} to the overall spurious asymmetry and a limit of 12×10^{-7} can be established for the photopeaks.

TABLE I. Dimensions and efficiencies of the p-type HPGe detectors used in the experiment.

Detector number	Diameter (mm)	Length (mm)	Efficiency (%) (relative to a 7.6 cm×7.6 cm NaI at 1.3 MeV)
1	55.7	56.2	29.7
2	56.0	57.9	30.3
3	55.8	54.8	28.0
4	54.1	58.0	27.9

E. Data acquisition

1. *Linear shapers*

The experiment was performed using four completely independent acquisition channels. Each channel consisted of a high throughput rate shaping amplifier followed by a fast analog to digital converter (ADC) equipped with analog backbias.

As far as the linear shapers are concerned, it has been shown[15] that the DL-RC shaper is the most effective in experiments where high throughput rates and good energy resolution are of primary interest. The output signals of the trapezoidal filter used in the parity violation experiment are shown in Fig. 6; the filter operates in conjunction with an HPGe detector and a ^{60}Co γ source is used. The throughput rate of the filter, defined as the rate of output signals which have not experienced pile up at the peak time (which in practice coincides with the measure time) is reported in Fig. 7 as a function of the input rate. From the figure a value of 14% to 20% can be inferred for the percentage of piled-up pulses for incoming rates in the range of 60–80 kcps. Energy resolution under in-beam condition was $\approx$3 keV at 1081 keV, to be compared with an energy resolution of $\approx$2 keV quoted by the manufacturer at 1333 keV, and 1 kcps rate, with a semigaussian filter working at 6 μs time constant.

2. *Analog to digital converters and direct memory increment*

The choice of ADC's was guided by their conversion time and by the settling time of the capacitor memory. Since 1024 channels are needed, taking into account the intensity distribution in the energy range of interest

FIG. 6. Output signals of the trapezoidal DL-RC shaper. X scale, 400 ns/div; Y scale, 0.5 V/div. A ^{60}Co source was used.

(800–1500 keV) it was found that by using analog backbias and proper settings of the lower and upper thresholds of the ADC, the 7420/G Silena ADC was the best suited for the purpose. In fact the "mean conversion dead time" after the risetime protection comes out to be $\approx 1.2\ \mu$s. On the other hand, risetime protection as short as 1 μs can be used in connection with pulses like those shown in Fig. 6, so that the total dead time of the system, taking also into account the operation of direct memory increment, is confined to about 3 μs. Since the rate in the selected energy window comes out to be ≈ 15 kcps, a dead time of 4.5% per channel is inferred.

Data are stored via DMI operation in four Camac resident memories,[16] each of which is split into two subsections of 1024 channels, which were selected, one at a time, according to the sense of the polarimeter current. In Fig. 8(a) a typical spectrum referring to the energy region of interest is shown.

F. Measurement control and data acquisition

The inversion of the magnetization in the polarimeter and data acquisition were controlled by a Hewlett-Packard 2108 computer. The time pattern of the polarimeter current consisted in an 8 s starting period, with

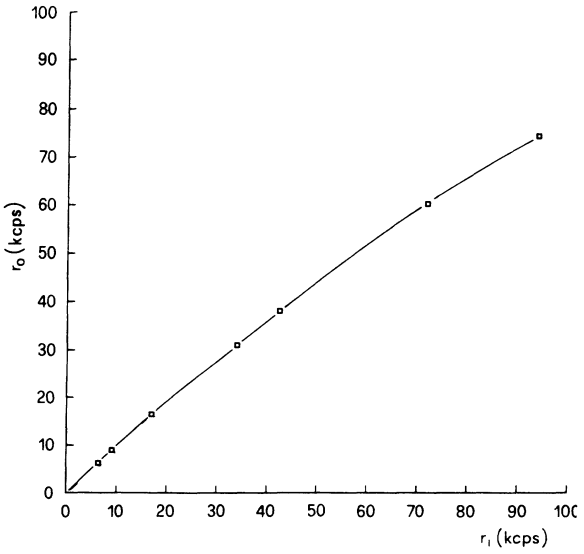

FIG. 7. Throughput rate of the trapezoidal DL-RC shaper. Errors of the experimental points are smaller than the symbols.

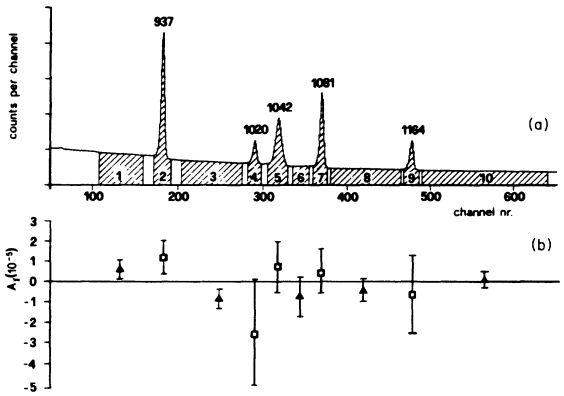

FIG. 8. (a) Typical spectrum; energies are in keV. (b) Asymmetries of the γ lines (from Table V column 2) and of background regions (from Table IV column 4).

current in one sense, followed by 19 periods of 16 s each of alternating current senses, ended with an 8 s period with current in the same sense as in the first one. The first 8 s period of the following cycle started with current reversed with respect to the preceding one. At the end of each period the ADC's inputs were inhibited and the inversion of the polarimeter current was started. Once the reaching of the steady value of the current had been sensed by a suitable circuitry, a new acquisition period started. The constancy of the induction flux changes toward the "+" and "−" steady values was verified by measuring them with a gated integrating amplifier and the result was acquired by the computer. At the end of each 320 s data acquisition period the contents of Camac memories were recorded on magnetic tape as eight spectra of 1024 channels each. In the following these spectra will be referred to as "single-cycle" spectra.

For possible checks in the offline analysis, every 8 s the values averaged over the last 8 s were recorded for beam current on target, current on the diaphragms, vacuum in the water jet chamber, accelerating voltage. Live and real times of the four acquisition channels were also recorded at the end of each cycle. Dead time values between 4% and 5% with a maximum difference among the four channels of 0.3% were measured.

A minor interference between the logic signals associated with the sense of the current in the polarimeter and the ADC backbias circuitry was identified giving rise to a small ($2-3\times10^{-3}$ channels) correlated shift of the centroids of the photopeaks. The effect of the shift has been investigated by simply correcting the spectrum for it and then calculating the new asymmetry values of the γ lines: the difference in the results came out to be less than 2×10^{-7}.

III. SYSTEMATIC EFFECTS

At the end of the experiment a total number of 49 100 single cycles had been recorded. Differences in the experimental situations in the two polarimeter phases due to fluctuations of the parameters of the measurement (unstable accelerator operation, tube kiks, beam intensity fluc-

tuations, radiation buildup in the circulating water, and so forth) are expected to be largely compensated for by the adopted time pattern of the polarimeter phases. Besides, as shown in Sec. II F, many of the experimental parameters are continuously monitored and recorded during data taking; in particular, the beam current deposited on the last diaphragms gave an overall indication of accelerator instabilities. On the raw data of the 49 100 cycles, a preanalysis was performed and those cycles have been discarded when the current on diaphragms (see Fig. 2) was larger than 0.1% of the total current and/or the difference in the deposited charge in the two phases was found larger than 10%. This reduced to 46 054 the number of cycles used for the subsequent analysis.

Adding up these "single-cycle" spectra, eight spectra have been obtained which will be referred to as "total statistics" spectra. In order to preserve a reasonable energy resolution, each pair of "single-cycle" spectra belonging to the same detector, was shifted, when necessary, by an integer number of channels, before being added. This procedure does not introduce any correlation among the channel contents; however, in the "total statistics" spectra the FWHM of the γ lines other than the 1081 keV one, which was chosen as a reference for the shift, are slightly larger than the "single-cycle" spectra and the effect is obviously largest for the 937 keV line.

Apart from the asymmetry of the 1081 keV line searched for, spurious asymmetries could be induced either by instrumental or physical mechanisms. Therefore, the first step in the analysis is to calculate the asymmetry of the whole of the "total statistics" spectra: in fact, this makes it possible to test with the largest available statistics the presence of any overall spurious asymmetry. A discussion about the choice of the asymmetry estimators is presented in Sec. IV; for the present calculation, we adopt the asymmetry estimator with which calculations are most easily done:[1,6]

$$A^R=\frac{1\ R-1}{4\ R+1}\ , \tag{1}$$

$$R=\frac{N_1^- N_2^+ N_3^- N_4^+}{N_1^+ N_2^- N_3^+ N_4^-}=\frac{N_1^{\uparrow} N_2^{\uparrow} N_3^{\uparrow} N_4^{\uparrow}}{N_1^{\downarrow} N_2^{\downarrow} N_3^{\downarrow} N_4^{\downarrow}}\ , \tag{2}$$

where N_k is the integral of the counts in the selected energy region and k is the detector index.

This estimator, when applied to the sum of background zones, to the sum of photopeak zones, and to the whole of "total statistics" spectra, leads to the results quoted in row 1 of Table II. From these results it is apparent that the asymmetries are all consistent with zero, within the errors. The result reported in the third column assesses an upper limit of 2.8×10^{-6} (67% confidence level) to the spurious asymmetry which is substantially smaller than the aimed accuracy ($\approx10^{-5}$) of the measurement for the 1081 keV line.

A study of the asymmetries induced by instrumental mechanisms shows that the expected associated contribution will be at most a fraction of the limit given above. Instrumental asymmetries, connected to different behaviors of the apparatus correlated with the two $(+,-)$ phases of the polarimeter ("synchronous systematic effects" in the following), are expected to influence both the continuum regions and the photopeaks almost in the same way.

A special effort has been dedicated by the various authors to point out the main synchronous systematic effects and to evaluate the amount of their contribution to the final asymmetries. The synchronous systematic effects which have been considered in the present work are the following.

(a) Gain and efficiency changes of the Ge detectors due to stray magnetic fields present at the detector's place.

(b) Crosstalk between logic and analog signals which may influence differently the response of the linear electronics in the two polarimeter phases.

(c) Magnetostriction.

(d) Displacement and intensity modulation of the beam at the target position (owing to the stray magnetic field along the beam path) and their interaction with dead time and pile-up.

As far as points (a) and (b) are concerned, results reported in Secs. II D and II F showed that their maximum contributions to the asymmetry of the lines are 12×10^{-7} and 2×10^{-7}, respectively. Point (c) was considered in Ref. 4 where a possible contribution to the asymmetry was found to be smaller than 7×10^{-7}. Since our polarimeter structure is similar to the one used in that experiment, the same limit is considered to be valid in our case.

Effects associated with point (d) are expected to be present, because of the synchronous displacement of the beam deduced from the stray field measurements. In the presence of a static offcenter of the beam spot with respect to the detectors and of differences in the dead time of the four channels, an asymmetry arises induced by a displacement of the beam spot and by a charge modulation correlated with the polarimeter phases. Using the estimator A^R defined by formulae (1) and (2) one finds

TABLE II. Calculations with different estimators of the asymmetry of the "total statistics" spectra. Estimators A^A and A^* are discussed in Sec. IV.

Asymmetry estimator	Background regions (10^{-5})	Photopeak regions (10^{-5})	Background plus photopeak regions (10^{-5})
A^R	-0.183 ± 0.155	0.062 ± 0.317	-0.136 ± 0.139
A^A	-0.183 ± 0.155	0.062 ± 0.317	-0.136 ± 0.139
A^*	-0.143 ± 0.155	0.099 ± 0.317	-0.097 ± 0.139

$$A^R_{\text{instr}} = \frac{A_Q}{4}(\tau_1+\tau_3-\tau_2-\tau_4) + \frac{\Delta X}{4L}\left[(\tau_1-\tau_3)+\frac{(l_1-l_3)}{L}\right] + \frac{\Delta Y}{4L}\left[(\tau_4-\tau_2)+\frac{(l_4-l_2)}{L}\right] . \quad (3)$$

In this expression

$$A_Q = \frac{Q^+-Q^-}{Q^++Q^-}$$

is the charge asymmetry in the two polarimeter phases, ΔX and ΔY are the full synchronous displacements of the beam along the directions of the detectors 1-3 and 2-4, respectively; τ_k is the fractional counting loss for the examined energy region in detector k, deriving from both the acquisition system dead time and pile-up; l_k is the distance between the beam spot and the estimated average interaction point (≈ 15 cm) in detector k; L is the average value of the four distances. An upper limit of 3 mm for differences l_1-l_3 and l_4-l_2 can be given on the basis of the mechanical tolerances of the water target assembly, of the polarimeter, and of the external and internal detector mountings. As reported in Sec. II the measured dead times of the acquisition system were about 5% for all the detectors. The pile-up loss differences among the various detectors can be obtained from the corresponding differences among the detector efficiencies, since the linear treatment of the signals is nominally the same for all detectors. Taking into account the average pile-up loss of 15% at 60 kcps, obtained by means of throughput rate measurements (see Fig. 7), one gets for the differences of counting losses

$$|\tau_1-\tau_3| \cong |\tau_4-\tau_2| \cong 1\times 10^{-2} ,$$
$$|\tau_2+\tau_4-\tau_1-\tau_3| \cong 2\times 10^{-3} .$$

The estimates of ΔX, ΔY, and A_Q are obtained by means of suitable estimators:[5,6]

$$\Delta X = \frac{L}{4}(D_{13}-1) \text{ with } D_{13} = \frac{T_1^+T_3^-}{T_1^-T_3^+} ,$$

$$\Delta Y = \frac{L}{4}(D_{24}-1) \text{ with } D_{24} = \frac{T_2^+T_4^-}{T_2^-T_4^+} ,$$

$$A_Q = \left[\frac{R_Q-1}{8}\right] \text{ with } R_Q = \frac{T_1^+T_2^+T_3^+T_4^+}{T_1^-T_2^-T_3^-T_4^-} ,$$

where T_k is the integral of the whole "total statistics" spectrum in detector k.[17] In Table III results for D_{13}, D_{24}, and R_Q are reported. No sizeable difference is observed for photopeaks and background zones: this result makes it possible to use the whole statistics for the evaluation of systematic effects. From data reported in Table III, column 3, one obtains

$$\Delta X = (-3.1\pm 0.3)\mu\text{m}$$
$$\Delta Y = (-0.4\pm 0.3)\mu\text{m} ,$$

TABLE III. Estimators of systematic effects associated with different phases of the polarimeter. For their definition, see text.

	Background regions (10^{-5})	Photopeak regions (10^{-5})	Background plus photopeak regions (10^{-5})
D_{13}	0.999 915 4± 0.000 008 7	0.999 926 6± 0.000 017 8	0.999 917 6± 0.000 007 8
D_{24}	0.999 987 4± 0.000 008 8	0.999 997 7± 0.000 018 0	0.999 989 4± 0.000 007 9
R_Q	0.999 831 1± 0.000 012 4	0.999 857 8± 0.000 025 4	0.999 836 2± 0.000 011 3

i.e., a displacement along the direction of detectors 1-3 is apparent, while a much smaller effect (if any) is present for the other direction. It is also to be noted that the value obtained for the displacement is consistent with the estimate (≈ 2 μm) based on stray field measurements. For the charge asymmetry a value of $A_Q = (-2.0 \pm 0.1)\times 10^{-5}$ is found; this value can be attributed to either a nonperfect compensation of uncorrelated beam current fluctuations, or to a synchronous modulation associated to the beam halo intercept by the diaphragms. Inserting in (3) the values of A_Q, ΔX, ΔY, and the already derived values of the dead time and of the static displacements (summing conservatively the effects), one obtains

$$A^R_{\text{instr}} \cong 2\times 10^{-7} .$$

Adding all the considered instrumental asymmetries one obtains a limit of 2.3×10^{-6}, within the experimental one of 2.8×10^{-6} reported in the second paragraph of this section.

Asymmetries of physical origin have already been investigated by different authors and, in particular, asymmetries have been considered associated with the following.

(a) Precession of aligned ^{18}F nuclei in the residual magnetic field at the beam spot position on the target.[1,2,4]

(b) Polarization rotation of linearly polarized γ rays from ^{18}F in the polarimeter.[4]

(c) Circularly polarized bremsstrahlung from electron capture or β^+ decay of ^{18}F.[1-4]

From the discussions on these points reported in the quoted literature, one cannot give a definite number for the expected asymmetries and for some of them values as large as 10^{-5} cannot be excluded.[1,2,4] However, all these effects are absent in photopeaks of lines belonging to the decay of $J=0$ levels, and an asymmetry may be induced only in the background underlying them because of Compton scattering and/or pile-up mechanism.

On the basis of this observation, the procedure to correct for possible physical effects is to evaluate the asymmetries of the background close to the lines (in particular the 1081 keV one) and correct accordingly the asymmetry of the energy region belonging to the photopeak.

IV. DATA ANALYSIS

In this section a detailed discussion is presented referring to the calculation of the asymmetry of energy regions (i.e., background or photopeak plus background regions) and of photopeaks in presence of finite background (subsections A and B, respectively). The various approaches followed in the literature are compared with respect to both their statistical properties and capability of compensating for systematic effects. A general procedure, already introduced in Ref. 5, for the calculation of the asymmetries which takes explicitly into account possible correlations in the data, is also discussed and applied for calculating the asymmetry value of the 1081 keV line. In the Appendix a comparison between photopeak asymmetries obtained by using the "total statistics" spectra and by combining the results of the "single-cycle" spectra is presented.

A. Evaluation of the asymmetry of selected energy regions

1. Comparison of the estimators A^R, A^*, and A^A

A preliminary analysis was performed with the aim of making the effect of possible physical asymmetry of the background evident. To check this point the asymmtry of the 10 energy zones shown in Fig. 8(a) was evaluated. Beside the estimator A^R, two more estimators (A^* and A^A) have been used for this analysis. These estimators have no particular advantage with respect to estimator A^R when asymmetries of energy zones are calculated; they are, however, better suited than A^R for calculating photopeak asymmetries and are introduced now for the sake of comparison.

Given a selected energy region, the "most efficient" estimator on purely statistical grounds (i.e., in the absence of systematic effects) should be

$$A^*=\frac{\sum_k \sum_{j=i_k}^{f_k} (n_{kj}^{\uparrow}-n_{kj}^{\downarrow})}{\sum_k \sum_{j=i_k}^{f_k} (n_{kj}^{\uparrow}+n_{kj}^{\downarrow})} ,$$

k is the detector index (1 through 4), i_k and f_k are the initial and final channels of the selected energy region of detector k, and n_{kj} is the content of channel j of detector k. This formula, in fact, corresponds to the weighted statistical average of single-channel asymmetries:

$$\alpha_{kj}=\frac{n_{kj}^{\uparrow}-n_{kj}^{\downarrow}}{n_{kj}^{\uparrow}+n_{kj}^{\downarrow}}$$

having the following estimator of the variance:

$$\sigma^2(\alpha_{kj})=\frac{1}{n_{kj}^{\uparrow}+n_{kj}^{\downarrow}} .$$

In Ref. 4 the arithmetic mean (A^A) of the four independent asymmetries calculated for each detector had been used

$$A^A=\tfrac{1}{4}\sum_k \frac{\sum_{j=i_k}^{f_k} (n_{kj}^{\uparrow}-n_{kj}^{\downarrow})}{\sum_{j=i_k}^{f_k} (n_{kj}^{\uparrow}+n_{kj}^{\downarrow})} .$$

With respect to compensation of systematic effects, estimators like A^R and A^A are better suited than A^*; in fact, estimator A^*, beside the spurious contributions given by expression (3) (which is common to all the three estimators), contains further terms, having the form

$$\begin{aligned} A^*_{\text{instr}} - A^R_{\text{instr}} &\cong A^*_{\text{instr}} - A^A_{\text{instr}} \\ &\cong \frac{A_Q}{4\eta}(\eta_2+\eta_4-\eta_1-\eta_3) \\ &\quad + \frac{\Delta X}{4\eta L}(\eta_1-\eta_3)+\frac{\Delta Y}{4\eta L}(\eta_4-\eta_2) , \end{aligned} \tag{4}$$

where

$$\eta_k=\frac{\epsilon_k}{L^2(1+\tau_k)}$$

represents the total detection efficiency of detector k and

$$\eta=\tfrac{1}{4}\sum_k \eta_k .$$

The presence of this effect has been checked by calculating the asymmetry of the whole "total statistics" spectra: in the last two rows of Table II the results for the asymmetry obtained applying A^* and A^A are reported; results obtained with A^R and A^A differ from each other by quantities smaller than the last reported digit; results obtained with A^* differ from the others by about 4×10^{-7}, as it can also be calculated from Eq. (4), using the known values of A_Q, ΔX, ΔY, and η_k. The difference between A^* and A^R is a random variable and therefore it is necessary to verify that the associated standard deviation is sufficiently smaller than the observed difference, in order that the latter be significant. If one calculates this standard deviation one finds

$$\sigma(A^*-A^R)\cong\sigma(A^*)\left[\frac{\sum_k \frac{\eta_k}{\eta}\left[\frac{\delta\eta_k}{\eta}\right]^2}{4}\right]^{1/2} ,$$

where

$$\delta\eta_k=\eta_k-\eta .$$

From the known values of η_k one finds that $\sigma(A^*-A^R)\approx5\times10^{-8}$, much smaller indeed than the observed difference.

2. Calculation of the asymmetries with estimators A^R, A^*, and A^A, applied to "total statistics" and "single-cycle" spectra

In Table IV the asymmetry values are reported for five background and five photopeak regions (two FWHM wide), obtained with estimators A^R, A^A, and A^* applied

TABLE IV. Columns 2 and 3: asymmetry of the energy regions shown in Fig. 8(a) calculated with estimators A^R, A^A, and A^*. Column 4: estimated asymmetry A_B of the background underlying the corresponding peak. Column 5: fitted values of second moments of the standardized distributions of the 46 054 "single-cycle" asymmetries. The "single-cycle" asymmetries have been evaluated with estimator A^R. The expected Poissonian fluctuation of the width is 0.003.

Energy region	A^R and A^A (10^{-5})	A^* (10^{-5})	A_B (10^{-5})	Fitted width
1	0.55±0.47	0.59±0.47		1.000
2 (937 keV)	0.46±0.63	0.48±0.63	−0.05±0.35	1.000
3	−0.90±0.52	−0.82±0.52		1.002
4 (1020 keV)	−1.30±1.15	−1.32±1.15	−0.84±0.50	1.004
5 (1042 keV)	0.19±0.75	0.25±0.75	−0.81±0.69	0.999
6	−0.78±0.94	−0.72±0.94		1.000
7 (1081 keV)	0.48±0.77	0.48±0.77	−0.67±0.67	1.004
8	−0.45±0.50	−0.40±0.50		0.994
9 (1164 keV)	−0.69±1.11	−0.61±1.11	−0.20±0.34	0.996
10	0.19±0.41	0.26±0.41		0.998

to "total statics" spectra. In column two of the table results obtained with estimators A^R and A^A are reported together as they differ by quantities smaller than the last reported digit. Asymmetries evaluated with A^* differ from those obtained with A^A and A^R by a small fraction of the standard deviation and this difference is due to two almost equal effects: the contribution given by Eq. (4) and the statistical fluctuation $\sigma(A^*-A^R)$ already discussed. The results of Table IV confirm anyway the substantial equivalence of all three approaches. Figure 8(b) shows the results for the background zones (estimators A^A and A^R), each below the corresponding energy region [Fig. 8(a)].[18]

The asymmetries for the same energy regions were also calculated as weighted statistical averages of the "single-cycle" asymmetries: for all the estimators the results coincide with the ones reported in Table IV. Standardized distributions of "single-cycle" asymmetries (i.e., distributions of the "single-cycle" asymmetries divided by their standard deviation calculated following the pure poissonian statistics), grouped in classes of 0.005 were sorted for all the energy zones (estimator A^R). By fitting these distributions with zero-centered Gaussian functions, the results shown in the fourth column of Table IV were obtained. The fitted widths, equal to unity within the expected uncertainty of $\sqrt{(1/2N)}=0.003$, where N (in the present case $=46\,054$) is the number of analyzed cycles, confirm that any source of fluctuation different from Poissonian origin gives negligible contribution. In particular, this result shows that the absence of significant systematic effects observed in the "total statistics" spectra does not derive from a cancellation, in the course of the measurement, of sizeable effects.

The results reported in column 2 of Table IV and shown in Fig. 8(b) have been used to have an estimate of the background asymmetry in the photopeak regions. Column 4 of Table IV contains the value of the asymmetry of the background underlying the peaks, extracted by means of a linear interpolation from the asymmetry of the closest background zones.

B. Evaluation of the asymmetry of photopeaks in presence of background

1. *Definition of the estimators A_P^R, A_P^π, A_P^A, and A_P^**

Different approaches have been followed for calculating the asymmetry of the photopeak of a γ line standing on a possibly polarized background.

Let us first discuss the procedure adopted in Ref. 2 and, for the case of four detectors, in Refs. 1 and 6: the asymmetry of the energy zone corresponding to the line of interest is calculated by means of estimator A^R and, once the asymmetry A_B of the underlying background is estimated from the neighboring zones, the asymmetry of the photopeak is evaluated as:[2,19]

$$A_P^R=\frac{1}{1-f}A^R-\frac{f}{1-f}A_B\ , \tag{5}$$

where f represents the ratio of background to total in the selected photopeak region. The results are somewhat dependent[6] on the choice of the line borders; besides, a procedure is also required to establish, for each γ line, the line borders which produce the minimum variance of the asymmetry; one finds that a reasonable choice is a region about 2 FWHM wide.[6]

Procedures like those described in Refs. 3 and 4 exploit better the information contained in the data and render the results quite insensitive to different choices of line borders: this is because the line asymmetry is obtained by weighting the information contained in each individual channel belonging to the line, with a weight proportional to the peak to total ratio of the channel itself.

The method developed in Ref. 3 is the following: the estimator $A_P^\pi(k)$ for each detector k, is searched for in the following form:

$$A_P^\pi(k)=\frac{\sum_i \pi_{ki}(n_{ki}^{\uparrow}-n_{ki}^{\downarrow})}{\sum_i \pi_{ki}(n_{ki}^{\uparrow}+n_{ki}^{\downarrow})}\cdot\beta_k\ , \tag{6}$$

where π_{ki} represents a set of weighting factors and β_k is a normalization constant; π_{ki} and β_k are determined by imposing a minimum for the variance of $A_P^{\pi}(k)$ and by requiring that A_P^{π} be an unbiased estimator of the true asymmetry. One finds

$$\pi_{ki}=\frac{F_{ki}}{F_{ki}+B_{ki}} ,$$

$$\beta_k=\frac{\sum_i \pi_{ki}(F_{ki}+B_{ki})}{\sum_i \pi_{ki}F_{ki}} ,$$

where $F_{ki}/(F_{ki}+B_{ki})$ represents the average peak-to-total ratio for channel i of detector k. This procedure can be applied to "single-cycle" spectra characterized by similar amplification, π_{ki} being determined from a reference spectrum obtained by summing these "single-cycle" spectra (up and down summed together). The final asymmetry is then obtained from the weighted statistical mean of these asymmetries. The background asymmetry A_B is corrected for by means of a term like the second one on the right-hand side of Eq. (5). This estimator will be applied in the Appendix to "single-cycle" spectra.

The procedure followed in Ref. 4 considers, for a given line, the single-channel asymmetries:

$$a_{ki}^{A}=\frac{n_{ki}^{\uparrow}-n_{ki}^{\downarrow}-2A_B b_{ki}}{n_{ki}^{\uparrow}+n_{ki}^{\downarrow}-2b_{ki}} ,$$

b_{ki} is the background associated to channel i, extracted from the average background of $\uparrow$ and $\downarrow$ spectra, by means of a linear fit connecting left and right background zones. The asymmetry $A_P^A(k)$ of the line in detector k is obtained as weighted statistical average of these single-channel asymmetries; the variance of the single-channel asymmetry is approximated by the expression

$$\sigma^2(a_{ki}^{A})=\frac{n_{ki}^{\uparrow}+n_{ki}^{\downarrow}}{(n_{ki}^{\uparrow}+n_{ki}^{\downarrow}-2b_{ki})^2} .$$

The procedure therefore neglects correlations among different channel asymmetries introduced by common terms b_{ki} and A_B. The line asymmetry A_P^A is then obtained as the arithmetic mean of the four detector asymmetries. It can be shown that the asymmetry calculated in this way contains a spurious instrumental contribution, which has the form of the right-hand side of Eq. (4), with the detector efficiency η_k replaced by the "total-to-peak" ratio of the examined region for this detector. This spurious contribution can be eliminated by introducing normalization constants in the spectra, which correct for the charge modulation and displacement of the beam, but this introduces a further correlation among all the single-channel asymmetries, even belonging to different detectors.

A procedure which explicitly takes into account the correlations and which can therefore be applied even when the condition of negligible covariance is not "*a priori*" easily predictable, has been introduced in Ref. 5. The single-channel asymmetry is defined as

$$a_{ki}^{*}=\frac{\rho_k^{\uparrow}(n_{ki}^{\uparrow}-A_B b_{ki}^{\uparrow})-\rho_k^{\downarrow}(n_{ki}^{\downarrow}+A_B b_{ki}^{\downarrow})}{\rho_k^{\uparrow}(n_{ki}^{\uparrow}-b_{ki}^{\uparrow})+\rho_k^{\downarrow}(n_{ki}^{\downarrow}-b_{ki}^{\downarrow})} ,$$

where (7)

$$\rho_k^{\uparrow}\cdot\rho_k^{\downarrow}=1 .$$

The normalization constants $\rho_k^{\uparrow},\rho_k^{\downarrow}$ are calculated for each detector k from the values of A_Q, D_{13}, and D_{24} reported in Table III. For each γ line, the multivariate normal distribution of the whole set of channel asymmetries a_{ki}^{*} (for all detectors together) is introduced and the estimator of the line asymmetry A_P^{*} is obtained following the Maximum Likelihood criterion [see, for instance, (20)]. The estimator is

$$A_P^{*}=\frac{\sum_{l,m} C_{lm}a_m^{*}}{\sum_{l,m} C_{lm}} , \quad (8)$$

where indexes l and m run over all the channels belonging to the line under study, for all detectors, and C_{lm} are the elements of the inverse of the covariance matrix associated to the set $\{a^{*}\}$. In cases where correlations among the channel asymmetries are negligible, the estimator A_P^{*} coincides with the weighted statistical average of the single-channel asymmetries.

2. *Calculation of the photopeak asymmetries with estimators A_P^A and A_P^{*} applied to "total statistics" spectra*

Calculations performed with estimator A_P^{*} are time consuming, as they require to handle relatively large covariance matrices: typically for a γ line, 20 channels for each spectrum are to be considered and consequently a covariance matrix of dimension 80×80 is to be inverted. Estimator A_P^{*} has been, therefore, applied only to the "total statistics" spectra, using for A_B the values reported in column 3 of Table IV. Results for the five γ lines are reported in column 2 of Table V; these are the values of the asymmetries reported in Fig. 8(b). The circular polarization P_γ (1081 keV) will be extracted from the asymmetry evaluated with this estimator.

In column 3 of Table V the results obtained with the estimator A_P^A applied to the "total statistics" spectra are also reported. It is apparent that the results are almost exactly the same: this confirms that in the present experiment, given the absence of significant systematic effects, even the estimator A_P^A gives correct results and that the refinements of the analysis introduced in A_P^{*} provide, in the present application, only minor corrections.

The asymmetries of Table V are obtained by choosing regions about 4 FWHM wide around the maximum of the relevant lines. As anticipated in the preceding subsection, a remarkable stability of the results with respect to different choices of the width of the energy region around the lines has been found for both the estimators A_P^{*} and A_P^A. For instance, if regions a factor of 2 narrower than those used in Table V are chosen, the estimated uncertainties remain the same within 1% and the

TABLE V. Asymmetries of γ lines shown in Fig. 8(a). The adopted value for the asymmetry of the 1081 keV line is that of column 2 (estimator A_P^*).

γ-line energy (keV)	Asymmetries A_P^* (10^{-5})	A_P^A (10^{-5})
937	1.16±0.86	1.14±0.86
1020	−2.55±2.63	−2.10±2.64
1042	0.80±1.25	0.69±1.28
1081	0.51±1.09	0.48±1.10
1164	−0.63±1.90	−0.60±1.90

asymmetry values are stable to within $\frac{2}{10}$ of the standard deviation. For the same range of selected regions, estimator A_P^R shows relative changes of the standard deviation of typically 10–20% and variations of the asymmetry, in some cases even as large as 100% of its standard deviation. As far as the values of the estimated uncertainties are concerned, one finds that those of estimator A_P^* are about 3–4% smaller than those of A_P^R (optimized with respect to the width).

V. CONCLUSIONS

Finally, the value of P_γ (1081 keV) is extracted from the corresponding asymmetry reported in Table V, that is

$$A_P^*\ (1081\ \text{keV})=(0.51\pm1.09)\times10^{-5}\ .$$

From this value and the measured analyzing power $S=(1.9\pm0.2)\times10^{-2}$, one finds $P_\gamma=(2.7\pm5.7)\times10^{-4}$. The weighted average of the experimental values obtained until now for the circular polarization of the 1081 keV γ ray[1–4] is

$$P_\gamma=(1.2\pm3.9)\times10^{-4}\ .$$

By using the relationship $|f_\pi|=(2.3\pm0.4)\times10^{-4}|P_\gamma|$ one finds an experimental limit for f_π (at one standard deviation confidence level): $|f_\pi^{\text{exp}}|<1.2\times10^{-7}$. This limit rules out a large part of the theoretical values predicted by different authors and, in particular, it is about four times smaller than the "best value" of DDH.[9]

However, recent theoretical works[10,11] revised the range of expected values of f_π, so reconciling theoretical predictions and experimental findings.

With respect to the constant used in the relation between f_π and P_γ, Kirchbach[12] critically revises the procedure used in Refs. 21 and 22 for deriving it from the analogous β^+ decay of ^{18}Ne and suggests that a value even 30% larger should be adopted; therefore, the experimental limit of f_π should be $|f_\pi^{\text{exp}}|<1.6\times10^{-7}$.

From the point of view of theoretical calculations of f_π, new results have been made recently available. Dubovik and Zenkin[10] performed a parameter-free calculation of the weak coupling constants in the frame of the standard model $SU(2)_L\times U(1)\times SU(3)_c$: a general agreement of their predictions with experimental results concerning many different systems is found. For what concerns f_π they calculate

$$f_\pi=f_\pi^F+f_\pi^{\text{NF}}=(1.6-0.3)\times10^{-7}=1.3\times10^{-7}\ ,$$

with a predominance of the factorizable part (F) with respect to the nonfactorizable one (NF); they also found that only neutral currents contribute to the strength of f_π. Their value of f_π comes out to be smaller than the previously calculated values (see, for instance, Ref. 7) and in particular 3.5 times smaller than the "best value" of DDH. This fact is explained by DZ on the basis of (1) the adopted values of the quark masses, which are larger than those used formerly; (2) the consistent use of the MIT bag model; (3) the choice of the low renormalization point of the operator H^{PNC} leading to negative value of f_π^{NF}. Besides, a range of possible values of f_π, arising from the uncertainty of the knowledge of quark masses, is given: $0.62\times10^{-7}<f_\pi<3.0\times10^{-7}$.

Moreover, a recent estimate of f_π by Desplanques[11] modifies the old range of possible values proposed by DDH and his new range is almost coincident with the one proposed by DZ:

$$0.5\times10^{-7}<f_\pi<3.5\times10^{-7}\ .$$

These new ranges of theoretical values of f_π as well as the "preferred value" of DZ come out to be in agreement with the experimental limit of f_π, either in the usually adopted version ($<1.2\times10^{-7}$) or following Kirchbach's suggestions ($<1.6\times10^{-7}$).

As a conclusion we may agree with these authors in saying that further nonambiguous insight on this subject could be obtained by substantially lowering the experi-

TABLE VI. Comparison among different estimators of the asymmetry. The data refer to a large subsample of the total statistics of the measurement. Columns 2 and 3 report the results of estimator A_P^* and A_P^A applied to the "total statistics" spectra, while columns 4 and 5 contain the results obtained by combining statistically the results of the "single-cycle" spectra calculated with estimators A_P^A and A_P^π.

γ line (keV)	"Total statistics" spectra A_P^* (10^{-5})	A_P^A (10^{-5})	"Single-cycle" spectra A_P^A (10^{-5})	A_P^π (10^{-5})
937	1.47±0.92	1.46±0.92	1.04±0.92	1.04±0.92
1020	−3.01±2.78	−2.89±2.78	−2.57±2.77	−2.90±2.78
1042	0.85±1.33	0.91±1.33	0.79±1.33	0.88±1.33
1081	−0.11±1.16	−0.13±1.16	−0.19±1.16	−0.18±1.16
1164	−1.17±2.03	−1.13±2.04	−0.93±2.03	−0.84±2.03

mental error on f_π. This is however, in our opinion, a very hard-to-reach goal in the case of ^{18}F, owing to the small analyzing power of the presently available polarimeters.

ACKNOWLEDGMENTS

The interest and the encouragement of Prof. P. G. Bizzeti and Prof. P. R. Maurenzig are warmly acknowledged. Thanks are also due to Prof. P. A. Mandò for critical suggestions.

APPENDIX

Comparison of photopeak asymmetries extracted from "single-cycle" and "total statistics" spectra.

Estimators A_P^A and A_P^π have been applied to the "single-cycle" spectra and then combined statistically; the results of these analyses are reported in Table VI. At the time when this comparison was made some tapes had been damaged and only 85% of the total statistics of the measurement could be sorted out. For the purpose of comparison, in Table VI are, therefore, reported the asymmetries calculated on this "total-but-smaller statistics" spectra with estimator A_P^* and A_P^A. From the table it is apparent that the results obtained by combining statistically the asymmetries of the "single-cycle" spectra agree very well for the 1081 and 1042 keV lines, with the asymmetries calculated on the "total statistics" spectra, regardless of the estimator used. The agreement is somewhat less good for the 937 keV line and this is due to the difference, in terms of resolution, between the "single-cycle" spectra and the "total statistics" spectra, as discussed at the beginning of Sec. III.

[1]S. A. Page *et al.*, Phys. Rev. C **35**, 1119 (1987).
[2]C. A. Barnes *et al.*, Phys. Rev. Lett. **40**, 840 (1978).
[3]P. G. Bizzeti *et al.*, Lett. Nuovo Cimento **29**, 167 (1980).
[4]G. Ahrens *et al.*, Nucl. Phys. **A390**, 486 (1982).
[5]M. Bini *et al.*, Phys. Rev. Lett. **55**, 795 (1985).
[6]H. C. Evans *et al.*, Phys. Rev. Lett. **55**, 791 (1985).
[7]F. Buccella, M. Lusignoli, L. Maiani, and A. Pugliese, Nucl. Phys. **B152**, 461 (1979).
[8]B. Guberina, D. Tadic, and J. Trampetic, Nucl. Phys. **B152**, 429 (1979).
[9]B. Desplanques, J. F. Donoghue, and B. Holstein, Ann. Phys. **124**, 449 (1980).
[10]V. M. Dubovik and S. V. Zenkin, Ann. Phys. **172**, 100 (1986).
[11]B. Desplanques, private communication.
[12]M. Kirchbach, J. Phys. G **13**, 135 (1987).
[13]M. Bini *et al.*, Nucl. Instrum. Methods Phys. Res., Sect. **A234**, 253 (1985).
[14]T. F. Fazzini *et al.*, Nucl. Instrum. Methods **192**, 287 (1982).
[15]N. Taccetti, Nucl. Instrum. Methods **225**, 118 (1984).
[16]M. Bocciolini, P. Calonaci, P. R. Maurenzig, and A. Perego (unpublished).
[17]In Ref. 5 a typing error (indexes 2 and 3 exchanged) and an incorrect expression ("diagonal of the polarimeter") rendered the discussion about this point very unclear.
[18]In Ref. 5 the asymmetry of energy zone No. 10 was erroneously reported as negative and so also was sketched in Fig. 2(b) of the same paper; the correct value is the one reported in Table IV of the present paper. The background asymmetry of zone No. 9 (the 1164 keV line) was correctly calculated, even in Ref. 5.
[19]H.-B. Mak, private communication.
[20]S. Brandt, *Statistical and Computational Methods in Data Analysis* (North-Holland, Amsterdam, 1976).
[21]W. C. Haxton, Phys. Rev. Lett. **46**, 698 (1981).
[22]E. G. Adelberger *et al.*, Phys. Rev. C **27**, 2833 (1983).

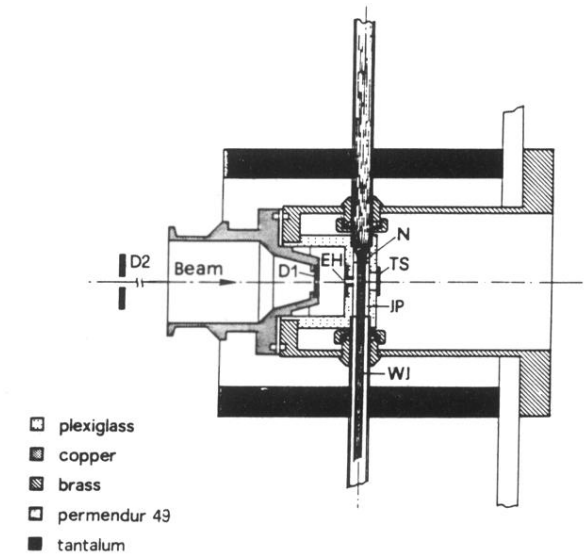

FIG. 2. Windowless water target. $D1$-$D2$, beam diaphragms; EH, entrance hole; TS, Tantalum stopper, N, nozzle; JP, water jet pipe; WJ, water jet.

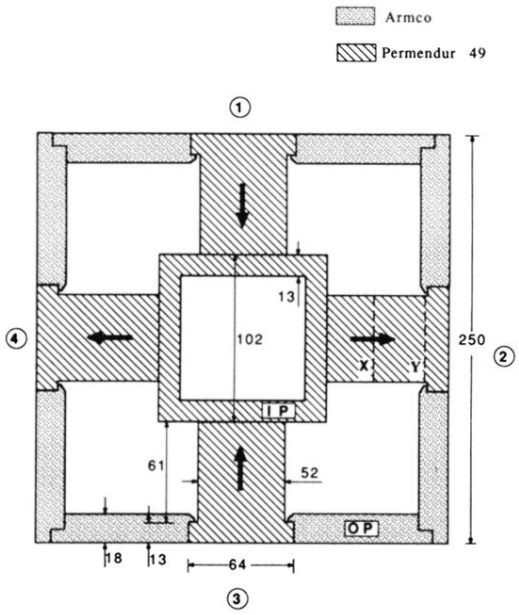

FIG. 4. Mechanics of the four-prong polarimeter. Dimensions are in mm.

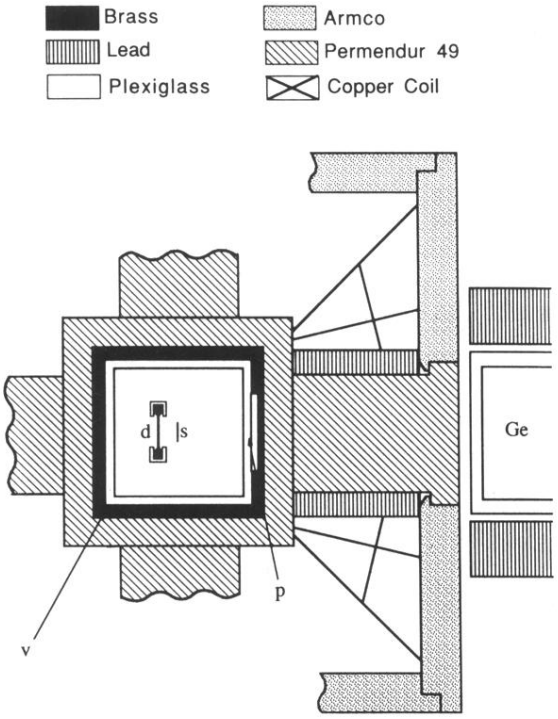

FIG. 5. Experimental setup for the measurement of the analyzing power of one prong of the polarimeter. *v*, vacuum chamber; *p*, Plexiglass lining; *s*, ^{22}Na β source; *d*, surface barrier silicon detector; Ge, HPGe detector.

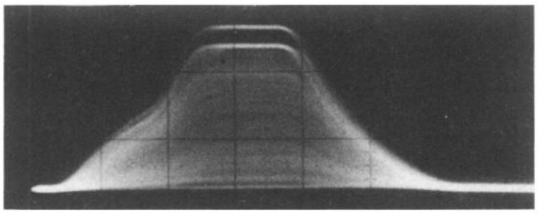

FIG. 6. Output signals of the trapezoidal DL-RC shaper. *X* scale, 400 ns/div; *Y* scale, 0.5 V/div. A ^{60}Co source was used.